Reversal of spin signals in anthraquinone based magnetic tunnel junctions

L. Chen[1,2†], J. Perrin[3†], I. Arbouch[5†], B. Dlubak[3], P. Seneor[3], R. Mattana[3], F. Godel[3], K. Sobnath[2], G. Wang[2], B. Janvier[2], P. Filloux[2], F. Mallet[2,4], C. Barraud[2], J. Cornil[5], C. Van Dyck[6], P. Martin[1*]*

[1] Université Paris Cité, CNRS, ITODYS, F-75006 Paris, France

[2] Université Paris Cité, CNRS, MPQ, F-75006 Paris, France

[3] Laboratoire Albert Fert, CNRS, Thales, Université Paris-Saclay, 91767 Palaiseau,

[4] Sorbonne Université, UFR925, 75005 Paris, France

[5] Laboratory for Chemistry of Novel Materials, Department of Chemistry, University of Mons

[6] Theoretical Chemical Physics group, Department of Physics, University of Mons

[*]Corresponding author. Email: pascal.martin@u-paris.fr & colin.vandyck@umons.ac.be

[†] These authors contributed equally.

KEYWORDS : molecular spintronic, graphene passivated electrodes, electrografted film, DFT.

Abstract: Molecular spintronics aims to control spin current transmission in magnetoresistive devices through molecular engineering. By tailoring the chemical structure of organic molecules atom by atom, chemistry offers a powerful route to design media for spin transport. A key milestone of the field is to tune spin polarization at ferromagnetic metal/molecule interfaces

according to their atomic-scale details. In parallel, research focuses on spin transport through functional molecules such as conformational switches and chiral systems. In this study, we investigate cross-conjugated molecular structures—specifically anthraquinone (AQ) oligomers—known to display destructive quantum interferences that may enhance current spin polarization. Experimental and theoretical data are presented for Co/graphene/AQ/Co spin-valve junctions fabricated via an electro-grafting method on graphene-protected electrodes. Observation of bias-dependent spin filtering, including spin polarization reversal, demonstrates a novel LUMO hybridization mechanism which can enable quantum spin-selective effects in future molecular spintronic devices.

INTRODUCTION

Molecular spintronics is a burgeoning field of research at the intersection between organic chemistry, spin physics and surface science[1–3]. The seminal idea behind the integration of organic molecules in spintronic devices was driven by the spin-OLED concept[4,5] whose first experimental demonstration was given later in 2012 by the group of Z. V. Vardeny[6]. An important foundational step was also accomplished around 2010 when it was demonstrated that the spin polarization, a quantity serving as a marker for spintronic device efficiency, could be crafted at the atomic scale at ferromagnetic metal/molecules hybrid interfaces[7–9], a.k.a. "spinterfaces"[6,10]. Since those early studies[3,11,12], controlling spin transport properties through interfaces has remained a highly active and fruitful research topic. Furthermore, it has been extended to complex interfaces including two-dimensional (2D) materials such as graphene[13], h-BN[14,15] and 2D semiconductors[16]. Beyond the extreme tunability of the hybrid ferromagnetic metal/molecules or even ferromagnetic metal/2D

materials/molecules interface properties[17], an intense research is also conducted towards the integration of functional molecules in devices. Recent discussions refer to chiral molecules and the associated chirality-induced spin selectivity effect [18–20]. Since the seminal work by the group of Naaman[21,22] in DNA molecules, other molecular systems like helicene[23,24] are under investigation for the generation of spin polarized current[25]. A recent review of this research is proposed in Ref. [26]. A second axis is related to cross-conjugated molecules[27–32]. Such molecular systems exhibit sharp anti-resonances at specific energies in their electronic transmission function, arising from destructive quantum interference (DQI). [33] Consequently, the charge current becomes strongly suppressed at these anti-resonance energies compared to linearly or even broken-conjugated systems. [34] Regarding spin transport, destructive interference may selectively filter one spin channel while allowing the opposite spin channel to transmit, as proposed in recent simulations. [35–37] Reported spin-filtering efficiencies approach 80%[35], and spin polarizations of up to ±60%[37] have been predicted from theoretical calculations.

These molecular structures or function could represent a significant breakthrough for the molecular spintronics and the predicted performance values rival those of the best MgO-based magnetic tunnel junctions reported to date for practical spintronics circuits[38–41]. However experimental results have remained elusive at the spintronic device scale and only concerned single molecule junctions made with vanadocene molecules[42]. In a recent paper[43], we have developed a new platform for the integration of the various molecular structure into organic spintronic functional devices. It has been demonstrated that electrografted organic films can be successfully integrated into spintronic devices by introducing direct CVD graphene which acts as a passivation layer, and serves as a platform for electrografting of organic molecules. The feasibility of this approach was demonstrated by focusing on model organic nitrobenzene oligomer chains. Spin

transport signatures in MR signal have been observed, confirming that spin sources remain intact during the novel fabrication process. Furthermore, the polarity of the spin signal can be reversed by altering the bias voltage, thereby modulating the tunneling of majority and minority spin carriers across the device, a phenomenon attributable to the coupling of the nitro moieties and the top electrode.

In this article, we report both experimental and theoretical data concerning magneto transport through Co/graphene/anthraquinone (AQ)/Co magnetic junctions. The electro-grafting of AQ cross-conjugated molecules based on our previous studies[27,32] provides high quality molecular layers for the study of their spin transport properties, while the Co spin source is preserved by a graphene overlayer during this wet integration process. We successfully fabricate spintronic devices by evaporating a Co top electrode and magneto measurement can be performed. We observe a positive and negative magneto resistance depending on the applied bias voltage. In addition, an intensive study at the Density Functional Theory (DFT) level was carried out and we are able to retrieve the same behavior of the experimental data. It demonstrates that the electron accepting properties of anthraquinone structure and the coupling strength of the two interfaces are responsible to this large reversal signal of Tunnel Magnetoresistance (TMR).

RESULTS

Fabrication and characterizations of the ~~quantum~~ molecular junctions

While diazonium electro grafting is well mastered for metallic electrodes[44] in various application[45,46], leading to high quality organic thin films of well-defined thicknesses[47,48], this wet

process remains incompatible due to the oxidation of the fragile materials used in spintronics, such as Ni and Co. This is particularly critical here as we aim to introduce functional AQ moieties in-between ferromagnetic spin sources. The quality of individual materials and of the interfaces is a key ingredient in spintronic devices. As previously reported, graphene is a perfect protection for ferromagnetic electrodes against oxidation[49,50]. This approach is therefore particularly relevant for investigating the anthraquinone layer in a spin valve configuration: Co/graphene layers/AQ film/Co hybrid magnetic junctions. The fabrication is described in Methods (Figure S1.A). Briefly, after a chemical vapor deposition step leading to graphene coverage of the bottom Co electrode, cyclic voltammetry is carried out to reduce the diazonium moieties and graft it on the Co/graphene electrode (Figure S1.B) [51,52]. After grafting no oxidation peak is observed on the X-Ray photo-electron spectrum of the modified electrode (Figure S1.C). The graphene layer still preserves the metallic nature of the surface of the Co spin source, which is instrumental for the observation of magnetoresistance. A high-resolution transmission electron microscope (HRTEM) image of the slice view done by Focus Ion Beam cutting is given in Figure S1 (inset). Distinct and well-defined graphene multilayers are clearly visible with a thickness of 2.5 nm on top of the amorphous cobalt layer, while a uniform 3 nm-thick anthraquinone film covers the graphene surface. The thickness of both layers is in good agreement with AFM measurement.

Magnetoresistive signals of the quantum organic junctions

In order to explore the spin properties of the modified graphene Co electrode, we further integrate it into a full spin valve structure (Figure S1.A). We use a Co top electrode as spin analyzer to study the polarization of the extracted current and the samples are measured with a standard DC current-voltage setup in a Montana C2 cryostat at 4.5 K. Further details related to the magneto-transport measurements can be found in supporting information. The measured current-voltage

characteristics under magnetic field (Figure 1.A) are highly non-linear and present asymmetric and visible features as highlighted by the 3 colored areas. These kinks are also present in control experiments where the Co electrodes are replaced by gold. They are attributed to electron-phonon interactions especially at low bias voltage.[30,53] The observed nonlinear I–V characteristics can be attributed to several factors related to the molecular and interfacial electronic structure. First, the alignment between the molecular frontier orbitals (particularly the LUMO in the case of AQ) and the Fermi levels of the electrodes plays a crucial role.[54,55] Under low bias, the weak coupling between the AQ orbitals and the electrodes limits the current, while at higher bias, the gradual alignment of the molecular orbital facilitates resonant tunneling, leading to nonlinear behavior. Second, interface barriers at the graphene/AQ and AQ/Co interfaces may introduce additional asymmetry in charge injection, further enhancing the nonlinearity.[56,57] In the following DFT calculation has been performed to further analyze the electronic structure of a model Co-Graphene-AQ-Co junction.

Several magnetoresistance measurements are carried out by varying the in-plane magnetic field and applying a fixed bias voltage at 4.5 K. For example, at V= −64 mV a negative magnetoresistance signal is observed and reaches 12% (Figure 1.B). The low-field coercive field around few mT is attributed to the thick bottom electrode (80 nm of Co) whereas the coercive field around 20 mT is attributed to the thinner top electrode (15 nm of Co). Possible contributions from anisotropic magnetoresistance (AMR) or tunneling anisotropic magnetoresistance (TAMR) are considered negligible in our devices. The typical AMR signal in Co electrodes is on the order of a few percent of their resistance (below 1 Ω), far smaller than the observed variations in the junction resistance. Furthermore, TAMR effects generally require highly crystalline interfaces, whereas both the Co electrodes and the organic layer in our junctions are polycrystalline. Consequently,

the measured MR response predominantly reflects spin-dependent tunneling across the molecular barrier.

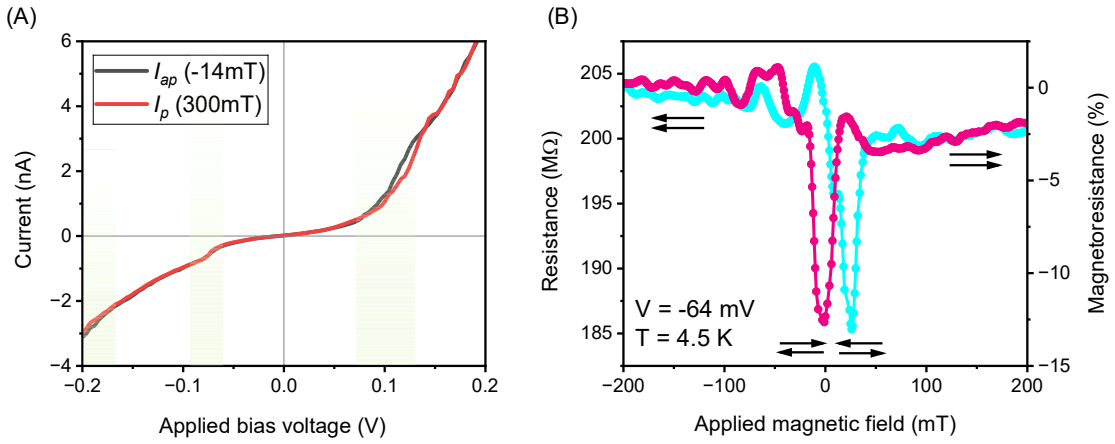

Figure 1: (A) Current-voltage characteristics of Co/Gr/AQ$_{3nm}$/Co sample measured at 4.5 K in the antiparallel state (black line) and in the parallel state (red line) of the Co magnetizations. The magnetic field is applied in the plane of both Co layers. (B) Negative magnetoresistive signal of −12 % measured at 4.5 K and for a bias voltage of −64 mV. The black arrows indicate the configuration of the magnetizations of both Co electrodes.

The complete evolution of the magnetoresistance with respect to the applied bias voltage is depicted in Figure 2.A. The black dots present the magnetoresistance extracted as usual from the contrast between I_P and and I_{AP}. The pink dots correspond to the direct measurements of magnetoresistance signals for several bias voltages as shown in Figure 1.B. A good agreement between both methods is observed. The small variation observed between the direct measurement and the calculated one can be explain by the fact that the position of the AP state in each MR loop may slightly shift when a bias is applied. As a result, the MR ratio extracted from the V–I curves of the P and AP states does not precisely reflect the overall MR ratio under different bias conditions. It should also be noted that fewer data points were obtained for the direct measurements

compared to the calculated ones. The magnetoresistance is shown to be highly asymmetric with respect to the applied bias voltage. It is mostly negative with a peak around 100 mV reaching −30 %. The magnetoresistance is however positive around zero bias voltage reaching +10%. Further details on the positive and negative TMR versus the applied magnetic field are shown in the supplementary information (Figure S2). Similar peculiar behavior has already been observed in spintronic devices based on 2D material (nanotube or graphene)[58,59] and electrografted layer[43].

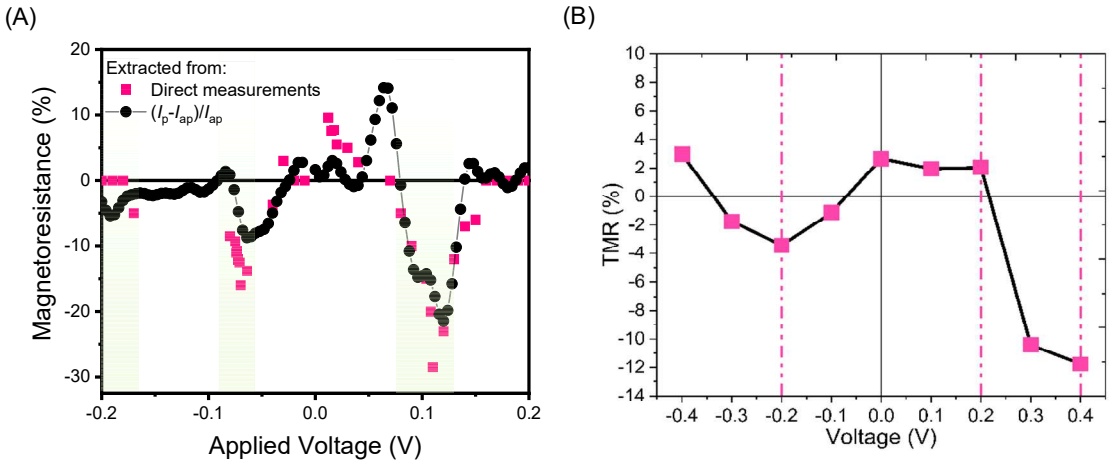

Figure 2: (A) measured TMR as a function of applied voltage extracted from R(H), in pink and extracted from I(V) curves, in black. (B) Calculated TMR as a function of applied voltage from the first principles calculation based on DFT. The solid black vertical line refers to the Fermi level.

To understand the origin of the apparent spin filtering effect across the Co/Gr/AQ/Co junction, first-principles calculations based on Density Functional Theory (DFT) have been performed. The simulated device is shown in Figure S3. The calculated TMR as a function of voltage is shown in Figure 2.B. The result is in qualitative agreement with the experimental TMR (Figure 2.A).

Charge-based devices with anthraquinone molecules have already been both experimentally and theoretically investigated[30,31,33,34]. An important feature from a quantum transport point of view is

the presence of a strong suppression of the charge current at specific energies related to anti-resonance in the transmission function. It was theoretically proposed that spin-polarized electrodes such as graphene nanoribbons[35] or even Ni by coupling with the anthraquinone molecule through chemical functional groups[37] could produce a lift of degeneracy between the two spin directions by 10 to 200 meV. However, the theoretical calculation reported here indicates that the coupling effect between the magnetic electrodes and the molecules is not as perceptible as in previous theoretical studies. It may be due to lower couplings with the magnetic contacts in comparison with previous theoretical suggestions. Indeed, the contacts involve a graphene separation layer on one side and physisorption on the other side. Nevertheless, the magnetization of the electrode has an effect on the molecular layer which rationalizes the experimental TMR curve as discussed below.

To interpret the variations observed on Figure 2.B, we relate the calculated transmission (Figure S4) to the electronic structure by focusing on the device density of states (DDOS). This latter is projected over the different junction components (cobalt electrodes, graphene and the two molecular fragments) and is reported in Figure 3 for the parallel (top panels) and antiparallel (bottom panels) spin configurations. Noteworthy, the bottom Co electrode is set to have a fixed magnetization, and this is the magnetization of the top Co electrode that gets switched in the calculations. For simplicity, we analyze the TMR curve by referring mainly to three points: +0.4 V (positive voltage), +0.2V (near Fermi level) and −0.2 V (negative voltage), as shown in Figure 2.A.

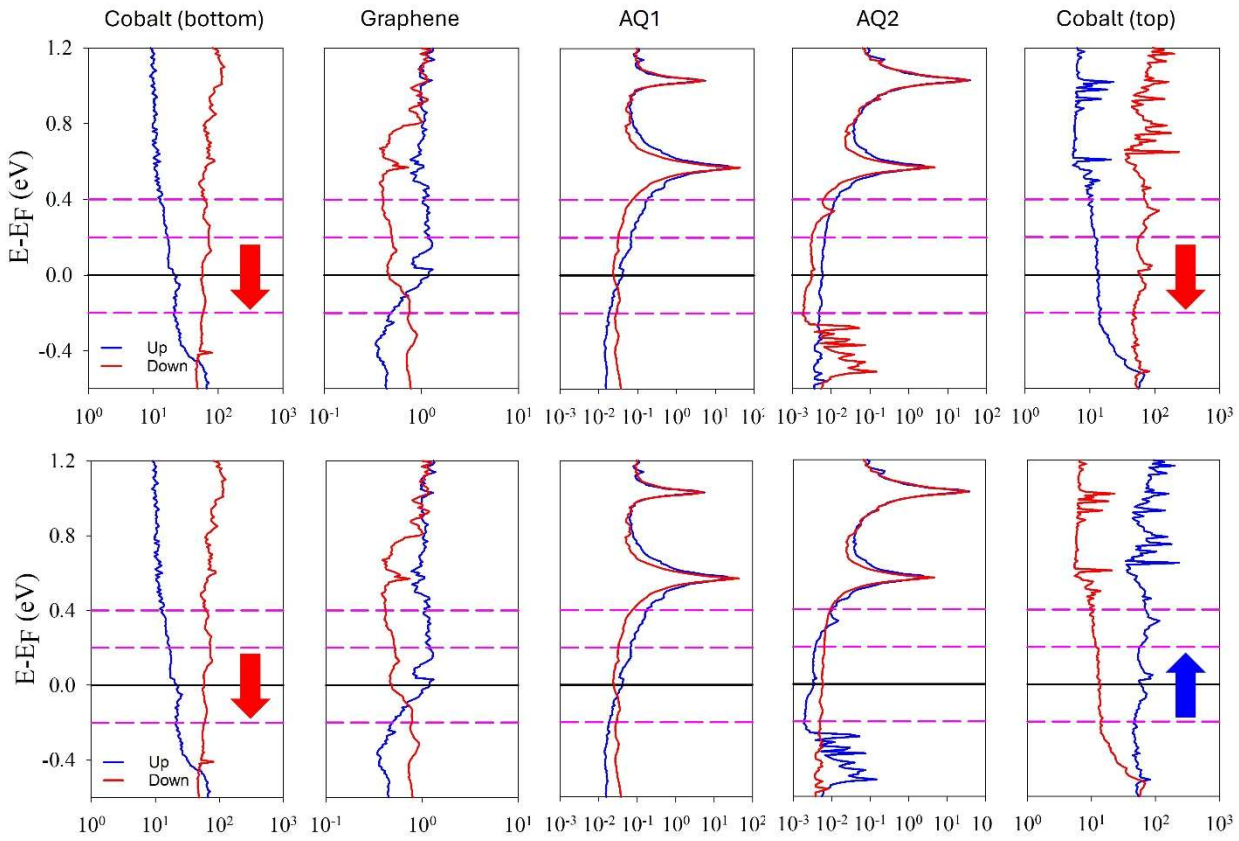

Figure 3: DOS projected over the bottom cobalt electrode, the graphene layer, the first unit (AQ_1), the second unit (AQ_2) and the top cobalt electrode. This is done for the parallel (top) and antiparallel (bottom) configurations as depicted by the relative orientation of the red and blue arrows. The solid black line indicates the Fermi level. The pink dashed lines serve as guide for the eyes to appreciate the situations at −0.2, +0.2 and +0.4 eV with respect to the Fermi level.

At +0.4 V, the TMR is clearly negative (Figure 2.B). This behavior is opposite to the prediction of Jullière's model for a spin unpolarized tunnel barrier directly contacted to cobalt electrodes. The role played by the molecule can be understood by analyzing the AQ LUMO orbital. It is located at +0.57 eV above the Fermi level and is delocalized over the AQ molecule with higher weight on the AQ_1 unit (see Figure S3). Consequently, the LUMO orbital couples better with the bottom Co/Gr electrode. In the PDOS, the LUMO peak broadening of the spin up channel is higher

compared to the spin down channel (see Figure 3). This observation applies to both AQ_1 and AQ_2 units. Importantly, the bottom cobalt electrode is primarily spin-down polarized. The LUMO spin polarization at these energies is thus opposite with respect to that of the bottom Co electrode. Moreover, the graphene layer polarization is also opposite to the bottom cobalt electrode. The molecular and graphene layers thus act as spin filters and, together with the cobalt substrate, act as a new effective electrode. The corresponding schematic is represented in Figure 4. In the parallel configuration, the bottom effective electrode becomes oppositely polarized to the top electrode. On the other hand, in the antiparallel configuration, the spin-polarizations of the top effective and bottom electrodes are the same (see Figure 4). This promotes a more efficient charge transport meaning that T_{AP} is larger than T_P and the sign of the TMR is negative for positive voltage. This reversed spin-polarization of the molecular LUMO peak and graphene layer could be due to a stronger electronic coupling with the s bands than the d bands of the bottom cobalt electrode. Indeed, the s and d bands exhibit opposite spin-polarizations in cobalt. The s band is spin-up polarized in energies up to 1 eV above the Fermi level, as shown in Figure S5.

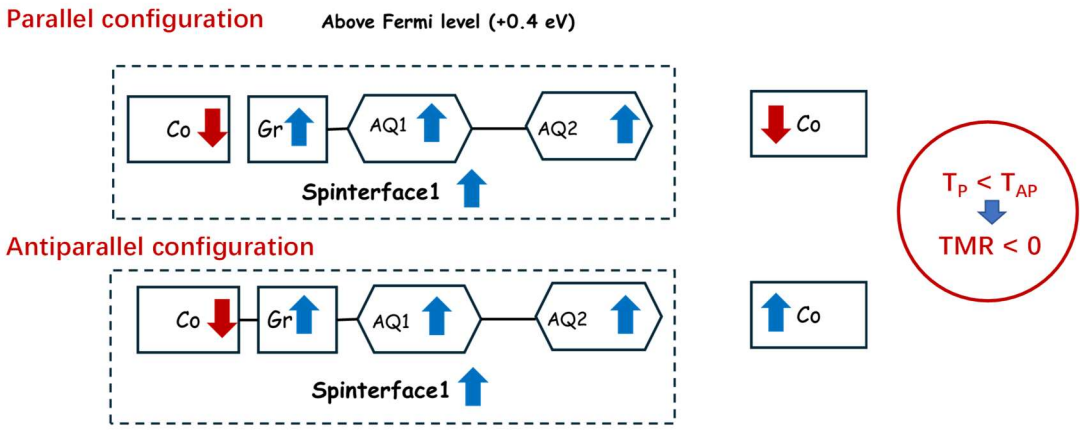

Figure 4: Sketch of the spin polarization at 0.4 eV above the Fermi level in parallel and antiparallel configurations. This rationalizes the negative TMR observed at positive biases.

As we approach the Fermi level, the TMR becomes positive. To elucidate this behavior, we examine the spin polarization of the various components in our device at +0.2 eV above the Fermi level (Figure 5). The degree of spin-polarization of graphene and AQ_1 tends to reduce as the Fermi level is approached. This naturally reduces the efficiency of the mechanism prevailing for positive biases that promotes a negative TMR. Moreover, the spin-polarization of AQ_2 at these energies becomes influenced by the top electrode polarization and systematically exhibits an opposite polarization relative to it. This observation indicates a significant electronic interaction between AQ_2 and the top contact despite the weak nature of van der Waals contacts. This interaction leads to the formation of a new spinterface between AQ_2 and the top electrode, ultimately resulting in the presence of two effective electrodes as sketched in Figure 5.A. Consequently, in the parallel (antiparallel) configuration, the effective top AQ_2/Co electrode promotes transport of spin up (down) electrons. This spin-polarization is compatible with the bottom effective electrode in the parallel configuration. On the other hand, the effective electrodes tend to inject oppositely spin-polarized electrons in the antiparallel configuration. Electron flow is then (dis-) favored in the (anti-) parallel configuration, and the sign of the TMR is positive.

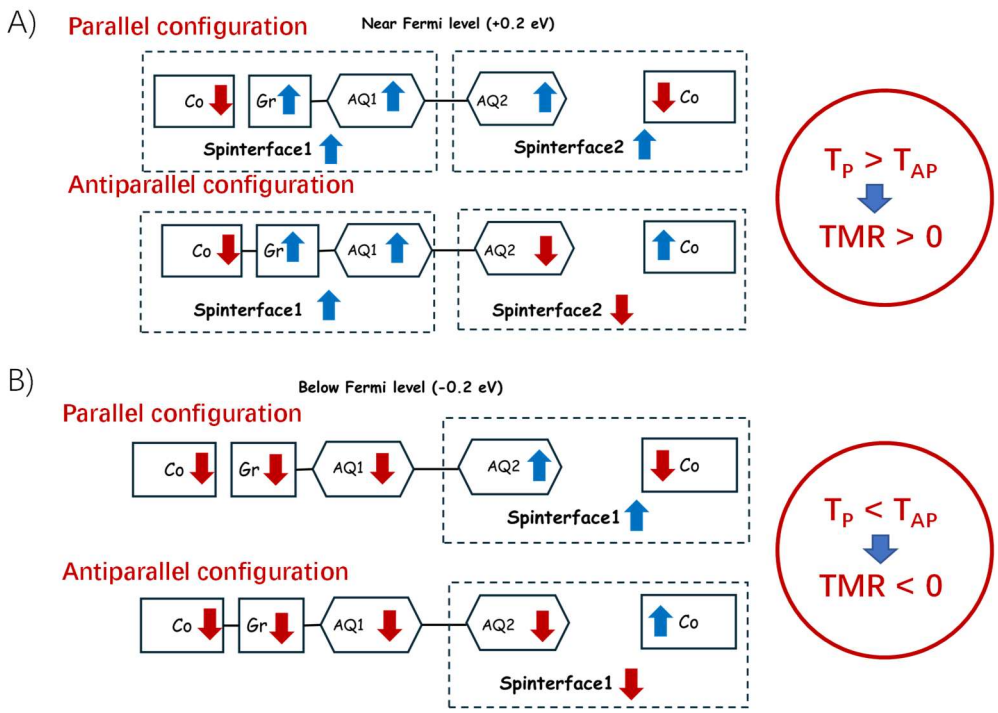

Figure 5: (A) Sketch of the spin polarization at the Fermi level in parallel and antiparallel configurations. This rationalizes the positive TMR observed at small biases. (B) Sketch of the spin polarization at −0.2 eV below the Fermi level in parallel and antiparallel configurations. This rationalizes the negative TMR observed at negative biases.

As we move from the Fermi level toward negative voltages, the TMR becomes negative. By analyzing the DOS across the different components of the device at −0.2 eV, we observe that both graphene and AQ_1 share the same spin polarization as the bottom Co electrode. Therefore, the opposite spin-filtering effect at the bottom contact disappears for negative voltages. However, at those energies, AQ_2 still systematically exhibits an opposite spin polarization relative to the top electrode (see Figure 3). This again suggests a significant electronic coupling between AQ_2 and the top cobalt electrode at those energies. Consequently, a spinterface remains located between the second unit and the top Co electrode. This spinterface exhibits an opposite (same) spin polarization relative to (as) the bottom electrode in the parallel (antiparallel) configuration (see Figure 5). As a

result, electron transport is favored in the antiparallel configuration and the sign of the TMR is negative.

In summary, the TMR is negative at both positive and negative voltages due to the formation of an effective bottom (Co/Gr/AQ_1) and top (AQ_2/Co) electrode, respectively, which acts as spin filters, resulting in a negative TMR. However, near the Fermi level, both effective electrodes (Co/Gr/AQ_1 and AQ_2/Co) contribute simultaneously, explaining the positive TMR. The molecular feature of AQ from a theoretical perspective is its electron accepting properties promoting a LUMO alignment. The broadening and inverse spin-polarization of this level in respect to the substrate electrode largely explains for the shape of the TMR curve, together with a significant electronic coupling at the van der Waals contact. Compared to the previously reported thick-film regime where destructive quantum interference (DQI) would dominate transport, the thinner junctions studied here would favor a regime governed by LUMO–electrode hybridization. The reduced thickness could enhance orbital coupling while limiting the full manifestation of DQI, as phase coherence may be constrained by the shorter transport path. As a result, the observed MR behavior would likely reflect spin-dependent tunneling through hybridized molecular orbitals rather than interference-driven conductance suppression.

CONCLUSIONS

Large and reversed magnetoresistive signals have been reported in Co/Gr/Anthraquinone/Co spin valve magnetic junctions. Firstly, we successfully electrografted anthraquinone-based organic film on graphene passivated cobalt electrode and preserve the ferromagnetic properties of the surface. The compact layer formed by electrochemical grafting allows us to deposit the second electrode to form the spintronic device. Magnetoresistance measurements have been performed

and surprisingly, we showed that the spin signal could be switched via the bias voltage tuning the MR sign. Supported by first-principles calculations, we proposed a microscopic mechanism including the simultaneous contribution of both interfaces which act as spin filter. Transport calculations indicate that the low lying of the LUMO level slightly hybridized with Cobalt electrodes qualitatively rationalizes the TMR, without clear exploitation of the quantum interference features of anthraquinone. While LUMO-mediated transport provides the primary explanation for bias-dependent TMR sign reversal, the cross-conjugated AQ backbone may retain its DQI potential in other device configurations, as evidenced by prior measurements on thicker films. Further investigations will be considered to fully investigate the proposed mechanism by characterizing other molecular acceptors. This work paves the way for accessing and exploiting spin-selective phenomena in molecular structures for spin valves applications.

ASSOCIATED CONTENT

Additional experimental details, materials, and methods, including additional figures as mentioned in the text

AUTHOR INFORMATION

Corresponding Author

*Pascal Martin (pascal.martin@u-paris.fr) and Colin Van Dyck (colin.vandyck@umons.ac.be).

Author Contributions

Conceptualization of experiments: PM, CB, BD
Methodology: LC, KS, BJ
Fabrication of Co/graphene spin source: JP, BD, FG
Magnetic experiments: LC, KS, PM, CB, FM
Theoretical calculations and analysis: IA, CVD, JC

SEM TEM investigations: GW, CB, LC

Supervision: PM, CB, BD

Writing – original draft: PM, CB

Writing – review & editing: CB, CVD, BD, PR, RM

ACKNOWLEDGMENT

The authors deeply thank D. Troadec from the IEMN in Lille for the focused ion beam cuts of the junctions and preparations of the HRTEM grids. They also acknowledge the Renatech French network. The authors also thank Dr. M. Rahimi, M. Nicolas, P. Filloux for their valuable contributions to the conception of the measurement setup and for their fruitful discussions. The Agence Nationale de la Recherche (France ANR-23-CE24-0009-01) are gratefully acknowledged for their financial support. The research in Mons is supported by the Belgian National Fund for Scientific Research (FRS-FNRS) via the project SPINFUN (Convention T.0054.20) and the EOS CHISUB project (No 40007495) and within the Consortium des Équipements de Calcul Intensif − CÉCI (Grant Number U.G.018.18), and by the Walloon Region (LUCIA Tier-1 supercomputer; Grant Number 1910247). J.C. is an FNRS research director.

REFERENCES

(1) Cinchetti, M.; Dediu, V. A.; Hueso, L. E. Activating the Molecular Spinterface. *Nat. Mater.* **2017**, *16* (5), 507–515. https://doi.org/10.1038/nmat4902.

(2) Forment-Aliaga, A.; Coronado, E. Hybrid Interfaces in Molecular Spintronics. *Chem. Rec.* **2018**, *18* (7–8), 737–748. https://doi.org/10.1002/tcr.201700109.

(3) Guo, L.; Gu, X.; Zhu, X.; Sun, X. Recent Advances in Molecular Spintronics: Multifunctional Spintronic Devices. *Adv. Mater.* **2019**, *31* (45), 1805355. https://doi.org/10.1002/adma.201805355.

(4) Xiong, Z. H.; Wu, D.; Valy Vardeny, Z.; Shi, J. Giant Magnetoresistance in Organic Spin-Valves. *Nature* **2004**, *427* (6977), 821–824. https://doi.org/10.1038/nature02325.

(5) Dediu, V.; Murgia, M.; Matacotta, F. C.; Taliani, C.; Barbanera, S. Room Temperature Spin Polarized Injection in Organic Semiconductor. *Solid State Commun.* **2002**, *122* (3–4), 181–184. https://doi.org/10.1016/S0038-1098(02)00090-X.

(6) Nguyen, T. D.; Ehrenfreund, E.; Vardeny, Z. V. Spin-Polarized Light-Emitting Diode Based on an Organic Bipolar Spin Valve. *Science* **2012**, *337* (6091), 204–209. https://doi.org/10.1126/science.1223444.

(7) Barraud, C.; Seneor, P.; Mattana, R.; Fusil, S.; Bouzehouane, K.; Deranlot, C.; Graziosi, P.; Hueso, L.; Bergenti, I.; Dediu, V.; Petroff, F.; Fert, A. Unravelling the Role of the Interface for Spin Injection into Organic Semiconductors. *Nat. Phys.* **2010**, *6* (8), 615–620. https://doi.org/10.1038/nphys1688.

(8) Atodiresei, N.; Brede, J.; Lazić, P.; Caciuc, V.; Hoffmann, G.; Wiesendanger, R.; Blügel, S. Design of the Local Spin Polarization at the Organic-Ferromagnetic Interface. *Phys. Rev. Lett.* **2010**, *105* (6), 1–4. https://doi.org/10.1103/PhysRevLett.105.066601.

(9) Javaid, S.; Bowen, M.; Boukari, S.; Joly, L.; Beaufrand, J.-B.; Chen, X.; Dappe, Y. J.; Scheurer, F.; Kappler, J.-P.; Arabski, J.; Wulfhekel, W.; Alouani, M.; Beaurepaire, E. Impact on Interface Spin Polarization of Molecular Bonding to Metallic Surfaces. *Phys. Rev. Lett.* **2010**, *105* (7), 077201. https://doi.org/10.1103/PhysRevLett.105.077201.

(10) Sanvito, S. Molecular Spintronics: The Rise of Spinterface Science. *Nat. Phys.* **2010**, *6* (8), 562–564. https://doi.org/10.1038/nphys1714.

(11) Bergenti, I.; Dediu, V. Spinterface: A New Platform for Spintronics. *Nano Mater. Sci.* **2019**, *1* (3), 149–155. https://doi.org/10.1016/j.nanoms.2019.05.002.

(12) Pandey, E.; Sharangi, P.; Sahoo, A.; Mahanta, S. P.; Mallik, S.; Bedanta, S. A Perspective on Multifunctional Ferromagnet/Organic Molecule Spinterface. *Appl. Phys. Lett.* **2023**, *123* (4), 040501. https://doi.org/10.1063/5.0166179.

(13) Zatko, V.; Dubois, S. M.-M.; Godel, F.; Galbiati, M.; Peiro, J.; Sander, A.; Carretero, C.; Vecchiola, A.; Collin, S.; Bouzehouane, K.; Servet, B.; Petroff, F.; Charlier, J.-C.; Martin, M.-B.; Dlubak, B.; Seneor, P. Almost Perfect Spin Filtering in Graphene-Based Magnetic Tunnel Junctions. *ACS Nano* **2022**, *16* (9), 14007–14016. https://doi.org/10.1021/acsnano.2c03625.

(14) Piquemal-Banci, M.; Galceran, R.; Godel, F.; Caneva, S.; Martin, M.-B.; Weatherup, R. S.; Kidambi, P. R.; Bouzehouane, K.; Xavier, S.; Anane, A.; Petroff, F.; Fert, A.; Dubois, S. M.-M.; Charlier, J.-C.; Robertson, J.; Hofmann, S.; Dlubak, B.; Seneor, P. Insulator-to-Metallic Spin-Filtering in 2D-Magnetic Tunnel Junctions Based on Hexagonal Boron Nitride. *ACS Nano* **2018**, *12* (5), 4712–4718. https://doi.org/10.1021/acsnano.8b01354.

(15) Dayen, J.-F.; Ray, S. J.; Karis, O.; Vera-Marun, I. J.; Kamalakar, M. V. Two-Dimensional van Der Waals Spinterfaces and Magnetic-Interfaces. *Appl. Phys. Rev.* **2020**, *7* (1), 011303. https://doi.org/10.1063/1.5112171.

(16) Yang, H.; Valenzuela, S. O.; Chshiev, M.; Couet, S.; Dieny, B.; Dlubak, B.; Fert, A.; Garello, K.; Jamet, M.; Jeong, D.-E.; Lee, K.; Lee, T.; Martin, M.-B.; Kar, G. S.; Sénéor, P.; Shin,

H.-J.; Roche, S. Two-Dimensional Materials Prospects for Non-Volatile Spintronic Memories. *Nature* **2022**, *606* (7915), 663–673. https://doi.org/10.1038/s41586-022-04768-0.

(17) Martin, P.; Dlubak, B.; Seneor, P.; Mattana, R.; Martin, M.; Lafarge, P.; Mallet, F.; Della Rocca, M. L.; Dubois, S. M. -M.; Charlier, J.; Barraud, C. Organic–Inorganic Hybrid Interfaces for Spin Injection into Carbon Nanotubes and Graphene. *Adv. Quantum Technol.* **2022**, *5* (6), 2100166. https://doi.org/10.1002/qute.202100166.

(18) Shang, Z.; Liu, T.; Yang, Q.; Cui, S.; Xu, K.; Zhang, Y.; Deng, J.; Zhai, T.; Wang, X. Chiral-Molecule-Based Spintronic Devices. *Small* **2022**, *18* (32), 2203015. https://doi.org/10.1002/smll.202203015.

(19) Naaman, R.; Waldeck, D. H. Spintronics and Chirality: Spin Selectivity in Electron Transport Through Chiral Molecules. *Annu. Rev. Phys. Chem.* **2015**, *66* (Volume 66, 2015), 263–281. https://doi.org/10.1146/annurev-physchem-040214-121554.

(20) Forment-Aliaga, A.; Gaita-Ariño, A. Chiral, Magnetic, Molecule-Based Materials: A Chemical Path toward Spintronics and Quantum Nanodevices. *J. Appl. Phys.* **2022**, *132* (18), 180901. https://doi.org/10.1063/5.0118582.

(21) Göhler, B.; Hamelbeck, V.; Markus, T. Z.; Kettner, M.; Hanne, G. F.; Vager, Z.; Naaman, R.; Zacharias, H. Spin Selectivity in Electron Transmission Through Self-Assembled Monolayers of Double-Stranded DNA. *Science* **2011**, *331* (6019), 894–897. https://doi.org/10.1126/science.1199339.

(22) Naaman, R.; Waldeck, D. H. Chiral-Induced Spin Selectivity Effect. *J. Phys. Chem. Lett.* **2012**, *3* (16), 2178–2187. https://doi.org/10.1021/jz300793y.

(23) Kettner, M.; Maslyuk, V. V.; Nürenberg, D.; Seibel, J.; Gutierrez, R.; Cuniberti, G.; Ernst, K.-H.; Zacharias, H. Chirality-Dependent Electron Spin Filtering by Molecular Monolayers of Helicenes. *J. Phys. Chem. Lett.* **2018**, *9* (8), 2025–2030. https://doi.org/10.1021/acs.jpclett.8b00208.

(24) Saleh, N.; Shen, C.; Crassous, J. Helicene-Based Transition Metal Complexes: Synthesis, Properties and Applications. *Chem. Sci.* **2014**, *5* (10), 3680–3694. https://doi.org/10.1039/C4SC01404A.

(25) Wolf, Y.; Liu, Y.; Xiao, J.; Park, N.; Yan, B. Unusual Spin Polarization in the Chirality-Induced Spin Selectivity. *ACS Nano* **2022**, *16* (11), 18601–18607. https://doi.org/10.1021/acsnano.2c07088.

(26) Bloom, B. P.; Paltiel, Y.; Naaman, R.; Waldeck, D. H. Chiral Induced Spin Selectivity. *Chem. Rev.* **2024**, *124* (4), 1950–1991. https://doi.org/10.1021/acs.chemrev.3c00661.

(27) Andrews, D. Q.; Solomon, G. C.; Goldsmith, R. H.; Hansen, T.; Wasielewski, M. R.; Duyne, R. P. V.; Ratner, M. A. Quantum Interference: The Structural Dependence of Electron Transmission through Model Systems and Cross-Conjugated Molecules. *J. Phys. Chem. C* **2008**, *112* (43), 16991–16998. https://doi.org/10.1021/jp805588m.

(28) Solomon, G. C.; Andrews, D. Q.; Goldsmith, R. H.; Hansen, T.; Wasielewski, M. R.; Van Duyne, R. P.; Ratner, M. A. Quantum Interference in Acyclic Systems: Conductance of Cross-Conjugated Molecules. *J. Am. Chem. Soc.* **2008**, *130* (51), 17301–17308. https://doi.org/10.1021/ja8044053.

(29) Valkenier, H.; Guédon, C. M.; Markussen, T.; Thygesen, K. S.; van der Molen, S. J.; Hummelen, J. C. Cross-Conjugation and Quantum Interference: A General Correlation? *Phys. Chem. Chem. Phys. PCCP* **2014**, *16* (2), 653–662. https://doi.org/10.1039/c3cp53866d.

(30) Bessis, C.; Della Rocca, M. L.; Barraud, C.; Martin, P.; Lacroix, J. C.; Markussen, T.; Lafarge, P. Probing Electron-Phonon Excitations in Molecular Junctions by Quantum Interference. *Sci. Rep.* **2016**, *6* (1), 20899–20906. https://doi.org/10.1038/srep20899.

(31) Salhani, C.; Della Rocca, M. L.; Bessis, C.; Bonnet, R.; Barraud, C.; Lafarge, P.; Chevillot, A.; Martin, P.; Lacroix, J.-C. Inelastic Electron Tunneling Spectroscopy in Molecular Junctions Showing Quantum Interference. *Phys. Rev. B* **2017**, *95* (16), 165431–165437. https://doi.org/10.1103/PhysRevB.95.165431.

(32) Hurtado-Gallego, J.; Davidson, R.; Grace, I. M.; Rincón-García, L.; Batsanov, A. S.; Bryce, M. R.; Lambert, C. J.; Agraït, N. Quantum Interference Dependence on Molecular Configurations for Cross-Conjugated Systems in Single-Molecule Junctions. *Mol. Syst. Des. Eng.* **2022**, *7* (10), 1287–1293. https://doi.org/10.1039/D2ME00074A.

(33) Markussen, T.; Schiötz, J.; Thygesen, K. S. Electrochemical Control of Quantum Interference in Anthraquinone-Based Molecular Switches. *J. Chem. Phys.* **2010**, *132* (22), 224104-224104–224106. https://doi.org/doi:10.1063/1.3451265.

(34) Rabache, V.; Chaste, J.; Petit, P.; Della Rocca, M. L.; Martin, P.; Lacroix, J.-C.; McCreery, R. L.; Lafarge, P. Direct Observation of Large Quantum Interference Effect in Anthraquinone Solid-State Junctions. *J. Am. Chem. Soc.* **2013**, *135* (28), 10218–10221. https://doi.org/10.1021/ja403577u.

(35) Saraiva-Souza, A.; Smeu, M.; Zhang, L.; Souza Filho, A. G.; Guo, H.; Ratner, M. A. Molecular Spintronics: Destructive Quantum Interference Controlled by a Gate. *J. Am. Chem. Soc.* **2014**, *136* (42), 15065–15071. https://doi.org/10.1021/ja508537n.

(36) Li, D.; Banerjee, R.; Mondal, S.; Maliyov, I.; Romanova, M.; Dappe, Y. J.; Smogunov, A. Symmetry Aspects of Spin Filtering in Molecular Junctions: Hybridization and Quantum Interference Effects. *Phys. Rev. B* **2019**, *99* (11), 115403. https://doi.org/10.1103/PhysRevB.99.115403.

(37) Qiu, S.; Miao, Y. Y.; Zhang, G. P.; Ren, J. F.; Wang, C. K.; Hu, G. C. Modulation of Hybrid Interface States and Magnetoresistance in Quantum Interference Systems via Functional Groups. *J. Magn. Magn. Mater.* **2021**, *537* (February), 168138. https://doi.org/10.1016/j.jmmm.2021.168138.

(38) Parkin, S. S. P.; Kaiser, C.; Panchula, A.; Rice, P. M.; Hughes, B.; Samant, M.; Yang, S.-H. Giant Tunnelling Magnetoresistance at Room Temperature with MgO (100) Tunnel Barriers. *Nat. Mater.* **2004**, *3* (12), 862–867. https://doi.org/10.1038/nmat1256.

(39) Tezuka, N.; Ikeda, N.; Sugimoto, S.; Inomata, K. Giant Tunnel Magnetoresistance at Room Temperature for Junctions Using Full-Heusler Co2FeAl0.5Si0.5 Electrodes. *Jpn. J. Appl. Phys.* **2007**, *46* (5L), L454. https://doi.org/10.1143/JJAP.46.L454.

(40) Yuasa, S.; Nagahama, T.; Fukushima, A.; Suzuki, Y.; Ando, K. Giant Room-Temperature Magnetoresistance in Single-Crystal Fe/MgO/Fe Magnetic Tunnel Junctions. *Nat. Mater.* **2004**, *3* (12), 868–871. https://doi.org/10.1038/nmat1257.

(41) Yuasa, S.; Djayaprawira, D. D. Giant Tunnel Magnetoresistance in Magnetic Tunnel Junctions with a Crystalline MgO(0 0 1) Barrier. *J. Phys. Appl. Phys.* **2007**, *40* (21), R337. https://doi.org/10.1088/0022-3727/40/21/R01.

(42) Pal, A. N.; Li, D.; Sarkar, S.; Chakrabarti, S.; Vilan, A.; Kronik, L.; Smogunov, A.; Tal, O. Nonmagnetic Single-Molecule Spin-Filter Based on Quantum Interference. *Nat. Commun.* **2019**, *10* (1), 5565. https://doi.org/10.1038/s41467-019-13537-z.

(43) Martin, P.; Dlubak, B.; Mattana, R.; Seneor, P.; Martin, M.-B.; Henner, T.; Godel, F.; Sander, A.; Collin, S.; Chen, L.; Suffit, S.; Mallet, F.; Lafarge, P.; Della Rocca, M. L.; Droghetti, A.; Barraud, C. Combined Spin Filtering Actions in Hybrid Magnetic Junctions Based on Organic Chains Covalently Attached to Graphene. *Nanoscale* **2022**, *14* (35), 12692–12702. https://doi.org/10.1039/D2NR01917E.

(44) Berisha, A.; Pinson, J.; Chehimi, M. M.; Podvorica, F. Electrode Surface Modification Using Diazonium Salts. In *Electroanalytical Chemistry: A Series of Advances*; CRC Press, 2015; Vol. 26.

(45) Deniau, G.; Zobrist, C.; Doizi, D.; Doublet, A.; Charrier, G. Recent Patents and Industrial Applications. In *Aryl Diazonium Salts and Related Compounds: Surface Chemistry and Applications*; Chehimi, M. M., Pinson, J., Mousli, F., Eds.; Springer International Publishing: Cham, 2022; pp 453–475. https://doi.org/10.1007/978-3-031-04398-7_23.

(46) Rabe, D. C.; Ho, U. K.; Choudhury, A.; Wallace, J. C.; Luciani, E. G.; Lee, D.; Flynn, E. A.; Stott, S. L. Aryl-Diazonium Salts Offer a Rapid and Cost-Efficient Method to Functionalize Plastic Microfluidic Devices for Increased Immunoaffinity Capture. *Adv. Mater. Technol.* **2023**, *8* (16), 2300210. https://doi.org/10.1002/admt.202300210.

(47) Fluteau, T.; Bessis, C.; Barraud, C.; Della Rocca, M. L.; Martin, P.; Lacroix, J.-C. C.; Lafarge, P.; Rocca, M. L. D.; Martin, P.; Lacroix, J.-C. C.; Lafarge, P. Tuning the Thickness of Electrochemically Grafted Layers in Large Area Molecular Junctions. *J. Appl. Phys.* **2014**, *116* (11), 114509. https://doi.org/10.1063/1.4896106.

(48) Pichereau, L.; López, I.; Cesbron, M.; Dabos-Seignon, S.; Gautier, C.; Breton, T. Controlled Diazonium Electrografting Driven by Overpotential Reduction: A General Strategy to Prepare Ultrathin Layers. *Chem. Commun.* **2019**, *55* (4), 455–457. https://doi.org/10.1039/C8CC08331B.

(49) Dlubak, B.; Martin, M.-B.; Weatherup, R. S.; Yang, H.; Deranlot, C.; Blume, R.; Schloegl, R.; Fert, A.; Anane, A.; Hofmann, S.; Seneor, P.; Robertson, J. Graphene-Passivated Nickel as an

Oxidation-Resistant Electrode for Spintronics. *ACS Nano* **2012**, *6* (12), 10930–10934. https://doi.org/10.1021/nn304424x.

(50) Joo, S.; Jung, K. Y.; Lee, B. C.; Kim, T.-S.; Shin, K. H.; Jung, M.-H.; Rho, K.-J.; Park, J.-H.; Hong, J.; Rhie, K. Effect of Oxidizing the Ferromagnetic Electrode in Magnetic Tunnel Junctions on Tunneling Magnetoresistance. *Appl. Phys. Lett.* **2012**, *100* (17), 172406. https://doi.org/10.1063/1.4704557.

(51) Kullapere, M.; Marandi, M.; Sammelselg, V.; Menezes, H. a.; Maia, G.; Tammeveski, K. Surface Modification of Gold Electrodes with Anthraquinone Diazonium Cations. *Electrochem. Commun.* **2009**, *11* (2), 405–408. https://doi.org/10.1016/j.elecom.2008.12.001.

(52) Bousquet, A.; Ceccato, M.; Hinge, M.; Pedersen, S. U.; Daasbjerg, K. Redox Grafting of Diazotated Anthraquinone as a Means of Forming Thick Conducting Organic Films. *Langmuir* **2012**, *28* (2), 1267–1275. https://doi.org/10.1021/la203657n.

(53) Bratkovsky, A. M. Assisted Tunneling in Ferromagnetic Junctions and Half-Metallic Oxides. *Appl. Phys. Lett.* **1998**, *72* (18), 2334–2336. https://doi.org/10.1063/1.121342.

(54) Pitié, S.; Seydou, M.; Dappe, Y. J.; Martin, P.; Maurel, F.; Lacroix, J. C. Insights on Asymmetric BTB-Based Molecular Junctions: Effect of Electrode Coupling. *Chem. Phys. Lett.* **2022**, *787* (July 2021), 139273. https://doi.org/10.1016/j.cplett.2021.139273.

(55) Rodriguez-Gonzalez, S.; Xie, Z.; Galangau, O.; Selvanathan, P.; Norel, L.; Dyck, C.; Costuas, K.; Frisbie, C. D.; Rigaut, S.; Cornil, J. HOMO Level Pinning in Molecular Junctions: Joint Theoretical and Experimental Evidence. *J. Phys. Chem. Lett.* **2018**, *9* (9), 2394–2403. https://doi.org/10.1021/acs.jpclett.8b00575.

(56) Nguyen, Q. van; Martin, P.; Frath, D.; Della Rocca, M. L.; Lafolet, F.; Barraud, C.; Lafarge, P.; Mukundan, V.; James, D.; McCreery, R. L.; Lacroix, J.-C. Control of Rectification in Molecular Junctions: Contact Effects and Molecular Signature. *J. Am. Chem. Soc.* **2017**, *139* (34), 11913–11922. https://doi.org/10.1021/jacs.7b05732.

(57) Nguyen, Q. V.; Frath, D.; Lafolet, F.; Lacroix, J. C.; Martin, P. Control of the Molecular Function through a Decoupling Unit. *J. Phys. Chem. C* **2024**, *128* (31), 13264–13270. https://doi.org/10.1021/acs.jpcc.4c02324.

(58) Bonnet, R.; Martin, P.; Suffit, S.; Lafarge, P.; Lherbier, A.; Charlier, J.-C.; Della Rocca, M. L.; Barraud, C. Giant Spin Signals in Chemically Functionalized Multiwall Carbon Nanotubes. *Sci. Adv.* **2020**, *6* (31), eaba5494. https://doi.org/10.1126/sciadv.aba5494.

(59) Rocha, A. R.; García-suárez, V. M.; Bailey, S. W.; Lambert, C. J.; Ferrer, J.; Sanvito, S. Towards Molecular Spintronics. *Nat. Mater.* **2005**, *4* (4), 335–339. https://doi.org/10.1038/nmat1349.